Acta Crystallographica Section B
Structural Science
ISSN 0108-7681

Charge-density analysis of 1-nitroindoline: refinement quality using free *R* factors and restraints

Bartosz Zarychta,[a,b] Jacek Zaleski,[a] Janusz Kyzioł,[a] Zdzisław Daszkiewicz[a] and Christian Jelsch[b]*

[a]Faculty of Chemistry, University of Opole, ul. Oleska 48, Opole 45-052, Poland, and [b]Laboratoire de Cristallographie, Résonance Magnétique et Modélisations (CRM2) CNRS, UMR 7036, Institut Jean Barriol, Faculté des Sciences et Technologies, Nancy University, BP 70239, 54506 Vandoeuvre-lès-Nancy CEDEX, France

Correspondence e-mail: christian.jelsch@crm2.uhp-nancy.fr

Received 7 January 2011
Accepted 7 April 2011

Nitramines and related *N*-nitro compounds have attracted significant attention owing to their use in rocket fuel and as explosives. The charge density of 1-nitroindoline was determined experimentally and from theoretical calculations. Electron-density refinements were performed using the multipolar atom formalism. In order to design the ideal restraint strategy for the charge-density parameters, *R*-free analyses were performed involving a series of comprehensive refinements. Different weights were applied to the charge-density restraints, namely the similarity between chemically equivalent atoms and local symmetry. Additionally, isotropic thermal motion and an anisotropic model calculated by rigid-body analysis were tested on H atoms. The restraint weights which resulted in the lowest values of the averaged *R*-free factors and the anisotropic H-atom model were considered to yield the best charge density and were used in the final refinement. The derived experimental charge density along with intra- and intermolecular interactions was analysed and compared with theoretical calculations, notably with respect to the symmetry of multipole parameters. A comparison of different refinements suggests that the appropriate weighting scheme applied to charge-density restraints can reduce the observed artefacts. The topological bond orders of the molecule were calculated.

1. Introduction

Compounds composed of a nitro group bonded to the ammonium N atom (nitramines and related *N*-nitro compounds) have attracted significant attention owing to their use in rocket fuel and as explosives (Williams, 1982). Growing interest in the development of such compounds is connected to the need to understand their energetic properties in relation to the structure and electron-density distribution features (Zhurova *et al.*, 2006; Pinkerton & Ritchie, 2003; Zhurova & Pinkerton, 2001). An area of particular importance is the weak intermolecular interactions since their rupture may provide a pathway for the shock initiation of energy release (Chen *et al.*, 2007). The chemistry of amino, nitroso and nitro compounds and their derivatives has been described by Wright (1969). Although they are well known, the synthesis, structure and properties of these compounds cause several difficulties. The NNO_2 group could be substituted by:

(i) two different aliphatic or aromatic groups ($RR'NNO_2$);

(ii) one substituent forming a cyclic configuration ($RNNO_2$);

(iii) one substituent joined by a double bond ($R{=}{=}NNO_2$).

The arrangement of atoms within the N_2O_2 group can be realized by:

(i) N—O—N—O of the furoxane aromatic ring,

(ii) N—NO_2 in *N*-nitramines and nitrimines, and

(iii) O—N—N—O as multidentate ligands in complexes for ε-caprolactone or lactide polymerization (Sarazin *et al.*, 2006).

Simple and small organic molecules of the nitramine class seem to be interesting models for investigations in the field of charge-distribution analysis. An interesting feature of the aromatic *N*-nitro compounds is their ability to rearrange under the influence of an acid, elevated temperature or on photolysis (Growenlock *et al.*, 1997). The migration is entirely intramolecular, *i.e.* the *N*-nitro group shifts three or five atoms from its original position while the remaining groups bind to the aromatic residue (Daszkiewicz *et al.*, 2002). The rearrangement of aromatic nitramines is an acid-catalyzed reaction. However, the acidity requirements are strongly dependent on the substrate. *N*-Methyl-*N*-phenyl-nitramine can be rearranged in dilute (0.1 *M*) sulfuric acid (White *et al.*, 1970), while the rearrangement of *N*-(2,3-dinitrophenyl)-nitramine only occurs in concentrated (78%) acid at room temperature (Ridd & Scriven, 1972). Such a difference suggests that the nitramino group is strongly influenced by the ring substituents (Daszkiewicz *et al.*, 2000). On the other hand, X-ray structural analyses of *N*-methyl-*N*-phenylnitramine and its ring-substituted derivatives indicated that the nitramine π-electron system is not conjugated with the aromatic sextet (Anulewicz *et al.*, 1993; Ejsmont *et al.*, 1998). Thus, the formally unshared electron pair on the amido nitrogen is delocalized towards the *N*-nitro group and does not interact with the π-electrons of the ring (Daszkiewicz *et al.*, 2000). Nevertheless, it seems that the interaction of the nitramino group with the aromatic ring is of inductive character even in molecules containing a positively charged ring, as in 4-(*N*-methylnitramino)-1-methylpyridinium bromide (Daszkiewicz *et al.*, 2002) and 4-(*N*-methylnitramino)-pyridine-1-oxide (Zaleski *et al.*, 1999). The conformation of the nitramino group is determined by the four-center π-orbital system. Derivatives of nitramine are important intermediates in the organic synthesis of pyridine, pyrimidine and *s*-triazine (Brzózka *et al.*, 1995). Moreover, owing to the presence of the N—N bond these compounds are also very active in photochemical reactions (Mialocq & Stephenson, 1986).

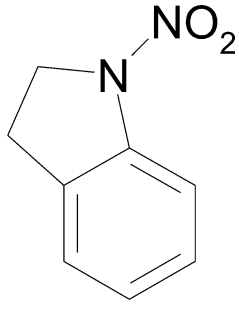

In this article the results of charge-density studies and *R*-free analyses (Brünger, 1992, 1993) of 1-nitroindoline are presented. *R*-free tests are widely used in macromolecular crystallography to assess the quality of the molecular structure. When the number of parameters refined in a crystal structure becomes too large with respect to the diffraction data set their values can become unrealistic, although the *R*-factors continue to decrease. The free *R*-factor is considered to be a better figure for structure refinement validation as its value increases when over-fitting of the experimental data occurs. In protein crystallography the resolution is generally lower than 1.5 Å and the number of observations is limited. Therefore, stereochemical restraints are necessary to obtain a reasonable crystal structure. The ideal weighting balance between the diffraction and stereochemical data can be determined using *R*-free tests.

In the case of charge-density analyses of small molecules, the resolution required is much higher ($d < 0.5$ Å) and stereochemical restraints are generally not necessary, except for hydrogen and disordered atoms. At the level of ultra-high resolution, the reliability of the refined charge density may be assessed by *R*-free analyses. For example, the diffraction data of good quality and resolution should enable the interaction electron density to be observed. Free *R*-factor analyses can determine if the charge density can be refined beyond the transferability approximation, *i.e.* should chemically equivalent atoms be constrained/restrained to have the same charge density. Two atoms are considered to be chemically equivalent when the number of neighbors and their chemical nature are the same up to the second level of connectivity. The geometrical characteristics (bond distances and angles) of the atoms also need to be similar. For O atoms the criterion is even stricter as the valence charge density is sensitive to the chemical nature of the bonded atoms up to the third connectivity shell. The atom equivalence constraints can be automatically generated by *MoPro* software, as described in Domagała & Jelsch (2009) and Zarychta *et al.* (2007).

2. Materials and methods

2.1. Synthesis and crystallization

1-Nitroindoline was prepared following the procedure described by Zaleski *et al.* (2001). Indoline and sodium hydride were heated in boiling toluene for 2 h under a nitrogen atmosphere. The mixture was cooled to room temperature, *n*-butyl nitrate was added and the suspension was stirred for 1 h at 298 K. Water was added, the layers were separated and the toluene layer was extracted with aqueous 10% sodium hydrogen sulfate to remove the unreacted amine. The solution was dried over anhydrous magnesium sulfate and evaporated under vacuum at 313 K. The residue was crystallized from ethyl ether/*n*-hexane, yielding colorless crystals melting at 363–366 K. Recrystallization from methylene chloride/*n*-hexane gave 1-nitroindoline (m.p. 362.5—363.5 K). Crystals were obtained by slow evaporation of a methylene chloride solution at room temperature. The compound is also light sensitive. A single crystal with dimensions 0.9 × 0.7 × 0.6 mm was used to collect the diffraction data.

2.2. Data collection and reduction

The 1-nitroindoline single-crystal X-ray diffraction experiment was performed at 90 K on an Xcalibur diffractometer, equipped with a CCD area detector and a graphite monochromator for the Mo $K\alpha$ radiation, with an Oxford Cryosystem N_2 gas-stream device. The reciprocal space was explored by ω scans. The low- and high-resolution reflections were measured with a radiation exposure time from 4 to 20 s, according to diffraction intensities. The detector was positioned 60 mm from the crystal. A total of 4589 frames were collected with a scan width of 0.75°. This procedure yields data collected up to a maximum resolution of $\sin\theta_{max}/\lambda = 1.33$ Å^{-1}.

The diffraction data reduction and empirical absorption correction of the compound studied were performed using *CrysAlis CCD* (Oxford Diffraction, 2002*a*; Oxford Diffraction, 2006). The final absorption correction factors for 1-nitroindoline are $A_{max} = 0.946$ and $A_{min} = 0.923$. The different sets of measured reflections were then merged and scaled using *SORTAV* (Blessing, 1995). For 1-nitroindoline 29 060 reflection intensities were collected resulting in 10 969 unique reflections, after averaging the Friedel pairs. Further details on the crystal data collection, processing and experimental conditions are given in Table 1.[1]

Table 1
Crystal and data collection statistics.

Crystal data	
Chemical formula	$C_8H_8N_2O_2$
M_r	164.15
Crystal system, space group	Triclinic, $P\bar{1}$
Temperature (K)	90
a, b, c (Å)	5.7913 (3), 8.2458 (6), 8.9223 (10)
α, β, γ (°)	116.823 (8), 104.589 (9), 91.602 (5)
V (Å^3)	362.99 (5)
Z	2
Radiation type	Mo $K\alpha$
μ (mm^{-1})	0.11
Crystal size (mm)	0.9 × 0.7 × 0.6
Data collection	
Diffractometer	Oxford Diffraction Xcalibur system
Absorption correction	Empirical (using intensity measurements), *CrysAlis RED*
T_{min}, T_{max}	0.923, 0.946
No. of measured, independent and observed [$I > 2.0\sigma(I)$] reflections	29 060, 8768, 7946
R_{int}	0.037
Completeness at $\sin(\theta_{max})/\lambda$	0.82
Completeness at $\sin(\theta)/\lambda = 0.92$ Å^{-1}	0.99
Average multiplicity	2.6
Refinement	
$R[F^2 > 2\sigma(F^2)]$, $wR(F^2)$, S	0.021, 0.024, 0.96
R_{merge}	0.012
No. of reflections	8768
No. of parameters	385
No. of restraints	203
H-atom treatment	Only H-atom coordinates refined
$\Delta\rho_{max}$, $\Delta\rho_{min}$ (e Å^{-3})	0.23, −0.20

Computer programs used: *CrysAlis CCD* (Oxford Diffraction, 2002*a*), *CrysAlis RED* (Oxford Diffraction, 2002*b*), *SHELXS*97, *SHELXTL* (Sheldrick, 2008), *MoPro* (Guillot *et al.*, 2001; Jelsch *et al.*, 2005).

2.3. Spherical-atom refinement

The 1-nitroindoline structure in space group $P\bar{1}$ was found to be the same as that determined at room temperature (Zaleski *et al.*, 2001). The structure was refined by a full-matrix least-squares method using *SHELXL*97 (Sheldrick, 2008). Lorentz and polarization corrections were applied. All H atoms were located from difference-Fourier synthesis. Non-H atoms were refined anisotropically and the displacement parameters for H atoms were freely refined. Details of the crystallographic refinement and statistics are listed in Table 2. The structure drawings were prepared using *SHELXTL*, *SHELXS*97 and *SHELXL*97 (Sheldrick, 2008).

2.4. Multipolar modeling

The electron-density refinements were performed with *MoPro* software (Guillot *et al.*, 2001; Jelsch *et al.*, 2005) using the Hansen & Coppens (1978) multipolar atom formalism. It allows modeling of the non-spherical part of the atomic electron density using the atom-centered multipole functions

$$\rho_{atom}(\mathbf{r}) = \rho_{core}(r) + P_{val}\kappa^3\rho_{val}^{sph}(\kappa r) + \sum_{l=0}^{l_{max}} \kappa'^3 R_l(\kappa' r) \sum_{m=0}^{l} P_{lm\pm} y_{lm\pm}(\theta, \varphi). \quad (1)$$

In the multipole formalism the core and spherical valence density of the atoms were calculated from Hartree–Fock wavefunctions expanded over Slater-type basis functions (Clementi & Roetti, 1974). For the multipolar terms, single-zeta radial functions R_l with energy-optimized Slater exponents were taken and kept fixed. An octupolar level of the multipole description was used for the C, N and O atoms, while for H atoms, the dipole level was applied.

2.5. Multipolar refinement strategy

The crystal structure resulting from the spherical atom modeling was used as input for the multipolar refinement *versus* diffraction intensities I_o. A first standard multipolar model refinement was performed using anisotropic displacement parameters for heavy atoms and isotropic ones for H atoms. The bond lengths for the H atoms were restrained to the standard neutron distances (Allen *et al.*, 1992) with an allowed standard deviation of 0.001 Å. The κ coefficients of the H atoms were initially restrained to the value of 1.160 (1) (Stewart *et al.*, 1965). The κ' coefficients of the H atoms, all bound to C atoms, were restrained to the values reported by Volkov *et al.* (2001), namely 1.20 (1). In the beginning stage of the multipolar refinement, several constraints on the charge density were applied:

(i) the multipole values of chemically equivalent atoms were constrained to be identical;

(ii) the kappa values for the two O atoms and for the chemically equivalent H atoms were constrained to have the same coefficients;

[1] Supplementary data for this paper are available from the IUCr electronic archives (Reference: PI5008). Services for accessing these data are described at the back of the journal.

Table 2
Crystallographic refinements statistics.

Atom model	Spherical	Multipolar
Refinement method	Full matrix least-squares on I	Full matrix least-squares on F
Data/restraints/parameters	10 969/0/141	8002/202/381
$\sin(\theta_{max})/\lambda$ (Å^{-1})	1.33	1.20
$I_o/\sigma(I_o)$ cut-off	3	1
Weighting scheme	$W_H = 1/[\sigma^2(I_o) + (0.0760P)^2]$, where $P = (I_o + 2I_c)/3$	$W_H = 1/\text{sigw}^2$ with $\text{sigw}^2 = [1.171\sigma^2(I_o) + 0.00074I_o^2]$
Goodness of fit on F	1.086	0.95
Final $R(I)$ indices $[I_o(I) > \sigma(I_o)]$	$R(F) = 0.0350$ $wR^2(I) = 0.1117$	$R(F) = 0.0250$, $wR^2(I) = 0.0480$
$\Delta\rho_{min}$, $\Delta\rho_{max}$ (e Å^{-3})	−0.32, 0.66	−0.20, 0.23

(iii) local symmetry constraints (mirrors) were applied to the multipolar charge density of the atoms.

During the refinement, all constraints were replaced by the related restraints. The weights of the restraints were set to the ideal values obtained from the *R*-free testing strategy. All multipolar refinements were carried out against the same strategy using the standard refinement procedure. U^{ij} and xyz variables of non-H atoms were refined using high-order reflections $s > 0.7$ Å^{-1} only. The whole resolution range was used for the refinement of the scale factor, xyz, U^{ij} valence and multipolar populations, κ' and κ. Only one type of parameter (xyz, U^{ij}, P_{val} ...) was allowed to vary in a refinement cycle. The different parameter types were refined successively and the whole procedure was iterated until convergence.

At the end of the first step of the multipolar refinement a rigid-body motion analysis was performed to derive the atomic displacement parameters (ADPs) for the H atoms. A translation–libration–screw (TLS; Schomaker & Trueblood, 1998) analysis was performed through the *SHADE* server (Madsen *et al.*, 2004). The ADPs of the H atoms were constrained to the anisotropic values obtained from the *SHADE* program. The multipolar refinement was then continued from the previous model. The κ and κ' coefficients for all non-H atoms were restrained to values derived from the charge density obtained from the theoretical data refinement with an allowed standard deviation of 0.01. The advantage of this approach (Kappa Restrained Refinement) has been discussed by Volkov *et al.* (2000).

At first, the multipolar refinement was performed with one scale factor, a weighting scheme $W_H = 1/\sigma^2(I_o)$ was applied and all the reflections were included (refinement SCA1). Analysis of the resulting set of reflections showed a $\langle F_o\rangle/\langle F_c\rangle$ ratio decreasing at high resolution down to 0.95. As demonstrated by Abrahams & Keve (1971), the weighted ΔF values should have a normal distribution. Plots of the final distribution against the expected distribution should have a slope of 1.0 and pass through the origin if the scale factor is correct. This was not the case, therefore, the refinement options and notably the weighting scheme was reconsidered (Zhurov *et al.*, 2008). The weak reflections were not well measured and underestimated in a plot of $\langle F_o\rangle/\langle F_c\rangle$ *versus* $\langle F_o\rangle/\langle \sigma F_o\rangle$, therefore, the data were cut at $I/\sigma_I > 1$. The diffraction data were also truncated at $s < 1.2$ Å^{-1} as the completeness in the shell $1.2 < s < 1.33$ Å^{-1} was only 29%. To ensure a more constant $\langle F_o\rangle/\langle F_c\rangle$ ratio, a polynomial scale factor of degree five as a function of reciprocal resolution s was used in the final refinement SCA5. The coefficients of the polynomial scale factor function were refined by the least-squares procedure in *MoPro* software, like the other parameters. The experimental sigma values were modified in the final refinement SCA5 to ensure a goodness-of-fit close to unity for all resolution and intensity shells: $\text{sigw}^2(I) = 1.17116\ \sigma^2(I_{obs}) + 0.00074\ I_{obs}^2$. The weighting scheme $W_H(I) = 1/\text{sigw}^2(I)$ was derived from these new sigma values. All the *R*-free analyses were perfomed in the conditions of refinement SCA5.

3. Charge-density analysis

The experimental static deformation electron density $\Delta\rho$ was computed from crystallographic modeling as the atomic superposition sum over the molecule

$$\Delta\rho = \sum\nolimits_{\text{atoms}} \rho_{\text{mul}} - \rho_{\text{sph}}, \qquad (2)$$

where the subscripts 'mul' and 'sph' represent the multipolar and spherical (neutral) atoms. The static maps correspond to the deformation electron density that would be observed for a molecule with immobile atoms and were computed directly using the refined values of xyz, P_{lm}, P_{val} and κ, κ' parameters describing the molecular charge density. Obtaining the static density maps necessitates the deconvolution of the thermal motion parameters U^{ij} from the electron density. This was performed with high-order refinements of the xyz and U^{ij} parameters of non-H atoms at $\sin\theta/\lambda > 0.7$ Å^{-1}.

The static electron density $\rho(r)$, topological analysis, bond-critical point (BCP) localization and intermolecular interaction energy calculations were performed using *VMoPro*, a properties visualization tool of the *MoPro* package (Jelsch *et al.*, 2005)

3.1. Free *R*-factor calculations

Since the conventional *R*-factor is not an absolutely objective indicator of model quality, *R*-free (Brünger, 1992, 1993) refinements were performed. The general principle of such a refinement consists of dividing the diffraction data into a large 'working' set and a small 'test' set which contains the free reflections. Free reflections are not used in the refinement, but the *R*-free value is computed after the refinement on that subset and is expected to decrease along with the conventional *R* factor. Prior to *R*-free refinements, the molecular structure was shaken: U^{ij} and xyz were modified by adding random numbers of r.m.s. value 0.003. This way, the shaken structure had no memory of the previous refinements and the free reflections could be considered as totally 'free'. The 0.003

Table 3
Geometric parameters: bond distances (Å) and valence angles (°) for non-H atoms of 1-nitroindoline.

O1—N2	1.2596 (4)	O1—N2—O2	124.25 (3)
O2—N2	1.2354 (3)	O1—N2—N1	119.87 (2)
		O2—N2—N1	115.87 (2)
N1—N2	1.3672 (3)	N1—C1—C2	107.23 (1)
N1—C1	1.4149 (3)	N1—C1—C6	129.82 (2)
N1—C7	1.5030 (3)	N1—C7—C8	104.92 (1)
		N2—N1—C1	126.03 (2)
		N2—N1—C7	120.72 (2)
		C1—N1—C7	112.15 (1)
C1—C2	1.4368 (3)	C1—C2—C8	112.10 (1)
C2—C3	1.3917 (3)	C1—C2—C3	120.03 (2)
C3—C4	1.4176 (3)	C1—C6—C5	116.19 (2)
C4—C5	1.4312 (3)	C2—C1—C6	122.95 (2)
C5—C6	1.4062 (3)	C2—C8—C7	102.91 (1)
C6—C1	1.4132 (3)	C2—C3—C4	118.05 (2)
C2—C8	1.5213 (3)	C3—C2—C8	127.87 (1)
C8—C7	1.5600 (3)	C3—C4—C5	121.31 (2)
		C4—C5—C6	121.46 (2)

r.m.s. value of the random shifts applied was two orders of magnitude larger than the estimated standard deviations of *xyz* and about ten times larger than the U^{ij} e.s.d.s. Therefore, the magnitudes of the perturbations are large enough so that the previous converged refinement has no effect.

As a single *R*-free value is subject to significant variation and depends on the set of free reflections used in the case of small molecules, *R*-free values were averaged over several different refinements. The (*hkl*) reflections were subdivided to define 20 working sets and their corresponding i = 1–20 complementary test sets consisting of 1 reflection out of 20 ($j = i, i + 20, i + 40 \ldots$). This subdivision allowed $N = 20$ refinements with a different test set for each. Using this strategy, a set of 20 refined $wR2F^{\rm work}$ and 20 $wR2F$-free factors were obtained and averaged. The average *R*-free value takes into account every reflection once and is therefore more stable and less dependent on the reflection tests sets used.

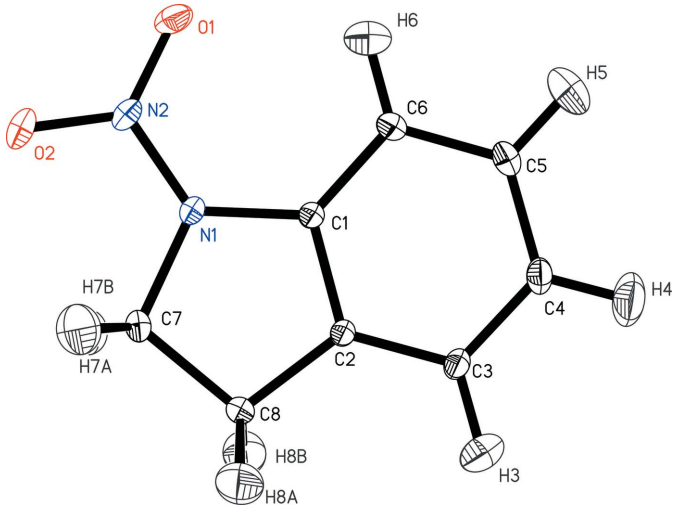

Figure 1
Molecular structure of 1-nitroindoline. Displacement ellipsoids are shown at the 50% probability level.

The quantity minimized in the refinements was a quadratic weighted sum over the reflections H and restraints

$$E = \sum\nolimits_{\rm H} W_{\rm H}(|I_{\rm obs}| - |I_{\rm calc}|)^2 + \sum\nolimits_{\rm restraints} W_{\rm R}(|R_{\rm target}| - |R_{\rm calc}|)^2. \quad (3)$$

The weight of the restraints is $W_{\rm R} = 1/\sigma^2(R_{\rm target})$, where $\sigma(R_{\rm target})$ is the allowed standard deviation.

A series of comprehensive refinements was carried out using different values of $\sigma(R_{\rm target})$ standard deviations ranging from 0.0001 up to 0.1 for the charge-density similarity restraints, which makes chemically equivalent atoms bear similar charge densities. The (κ, κ') coefficients, valence and multipolar populations were regrouped in these similarity restraints. Local symmetry restraints (*i.e.* one or two mirrors per atom) were also applied to the atomic multipolar charge densities and different weights were tested. The lowest values of the averaged *R*-free factors were considered to yield the best restraint model, which were then applied in the final refinement.

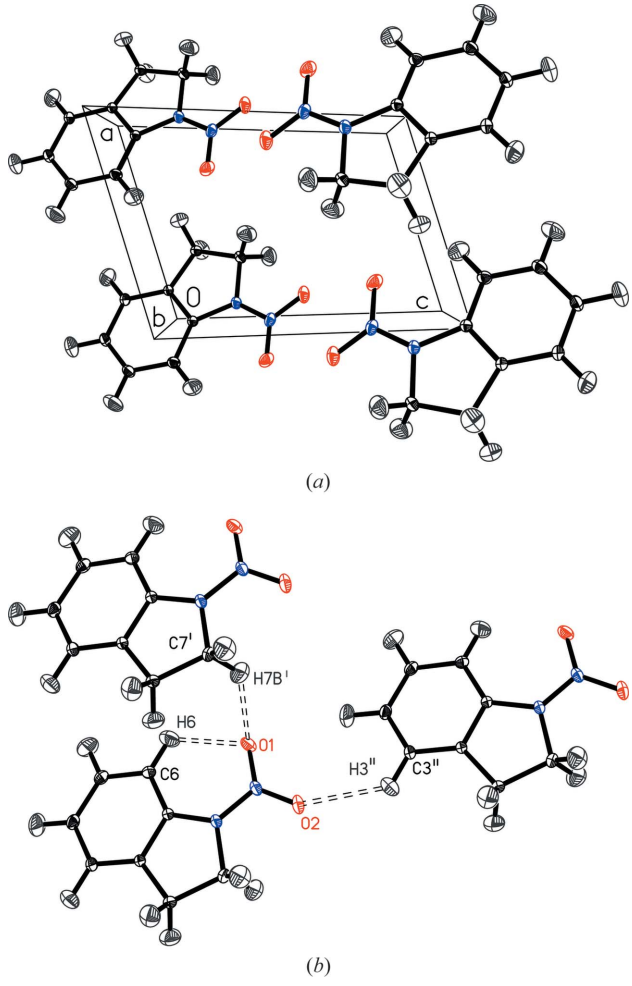

Figure 2
(*a*) Packing diagram and (*b*) hydrogen-bonding scheme of 1-nitroindoline. Displacement ellipsoids are shown at the 50% probability level. Symmetry codes: (i) $x, y + 1, z + 1$; (ii) $x - 1, y, z$.

Table 4
Geometrical characteristics (distances, Å, and angles, °) of the strongest hydrogen bonds in the 1-nitroindoline crystal packing.

D—H···A	$d(D$—H) (Å)	d(H···A) (Å)	$d(D\cdots A)$ (Å)	$\angle(DHA)$ (°)
C3—H3···O2^{i}	1.083	2.499	3.3395 (3)	133.6
C5—H5···O1	1.083	2.656	3.4361 (3)	128.5
C6—H6···O1	1.082	2.306	2.8779 (3)	111.1
C7—H7B···O1^{ii}	1.090	2.453	3.3363 (3)	137.2

Symmetry transformations used to generate equivalent atoms: (i) $x, -1+y, -1+z$; (ii) $1+x, y, z$.

3.2. Theoretical calculations

Periodic quantum calculations using *CRYSTAL*06 (Dovesi *et al.*, 2008) were performed. The molecular structure observed experimentally in the crystal was used as a starting geometry; optimization was performed with the density-functional theory (DFT) method (Hohenberg & Kohn, 1964) and with the B3LYP hybrid functional (Lee *et al.*, 1988) using the 6-31G(d, p) basis set (Hariharan & Pople, 1973). Upon energy convergence ($\sim 10^{-6}$), the periodic wavefunction based on the optimized geometry was obtained. The coordinates of all the atoms were optimized, but the unit cell was kept fixed. The option XFAC was used to generate a unique set of 18 404 theoretical structure factors (up to 1.2 Å^{-1} reciprocal resolution) from the computed electron density.

The charge density of the obtained theoretical structure was refined until convergence. The κ values of the H atoms were restrained to a value of 1.16 (3) and refined.

4. Results and discussion

4.1. Molecular and crystal structure

The structure of 1-nitroindoline has been previously reported by Zaleski *et al.* (2001). Since the previous experiment was performed at room temperature, some structural differences are observed. The bond lengths, angles and torsion angles of the 1-nitroindoline structure at 90 K (after the multipolar refinement) are given in Table 3. Compared with the structure at room temperature (Zaleski *et al.*, 2001) the unit-cell volume is reduced by 3%.

The structure of the molecule along with thermal displacement ellipsoids is depicted in Fig. 1. The geometry of the nitramino group is slightly changed in comparison to the room-temperature structure. The bond length which deviates most from the values at 295 K is N2—O1 [Δ = 0.034 (2) Å], while the second N2—O2 bond differs only by 0.004 (2) Å. This is due to the strengthening of the intramolecular O1···H6—C6 and intermolecular C7—H7B···O1^{ii} hydrogen bonds in the low-temperature phase. The presence of the hydrogen bond also influences the N1—C1—C6 valence angle, which is decreased by 1.5 (2)° at low temperature. The values of the torsion angles around the N1—N2 bond [O1—N2—N1—C1 = 12.48 (2) and O1—N2—N1—C7 = 179.51 (2)°] show that the C1 atom is slightly out of the plane of the nitro group and the N1 atom is pyramidal. The nitramino group is slightly twisted with respect to the aromatic ring plane [N2—N1—C1—C6 = −7.12 (2)°], which confirms the fact that the π-electron system of the nitramino group should not be seriously disturbed by the aromatic ring. There are no other critical differences among structures obtained from data collected at room and low temperature.

The molecules in the crystal are arranged in the *ac* plane and connected to each other (head to tail) by weak C3—H3···O2 and C7—H7B···O1 hydrogen bonds (Fig. 2, Table 4).

There is an intermolecular contact among the nitro groups of molecular stacks (Fig. 3). The intermolecular O2···O2 distance between two neighboring molecules related by an inversion center is 2.831 (3) Å, while the O2···N2 distance is 2.906 (3) Å. These distances are smaller than the accepted sum of the van der Waals radii. This is usually observed in

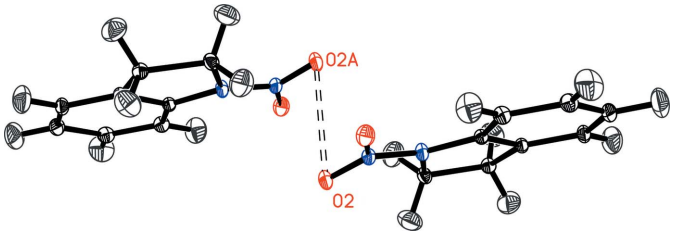

Figure 3
O···O interaction in 1-nitroindoline crystals. Displacement ellipsoids are shown at the 50% probability level. Symmetry code between the two molecules: $2-x, 2-y, 1-z$.

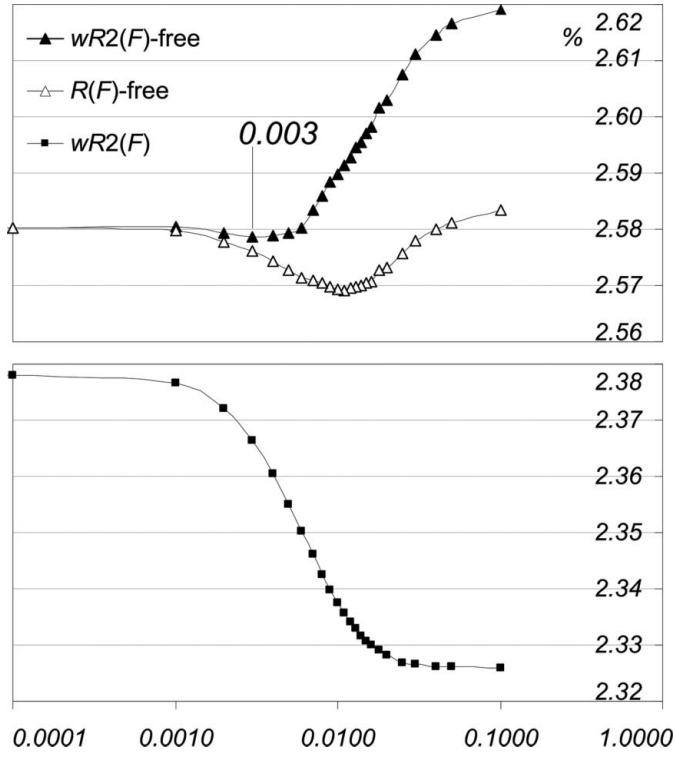

Figure 4
*wR*2(*F*), *R*(*F*)-free and *wR*2(*F*)-free values as a function of the allowed standard deviation applied to the charge-density symmetry restraints.

nitro compounds when two molecules are involved in a complex hydrogen-bonding scheme, rarely as a 'standalone' O···O contact (Gavezzotti, 2010). In the current crystal study the interaction can also be due to the presence of an attractive electrostatic contact between N2 and O2 atoms as a result of the resonance contribution in the nitro group. A critical point was found on the O2···O2 path, but not for the O2···N2 interaction. In connection with the steric repulsion of the O atoms, the nitro group is slightly twisted.

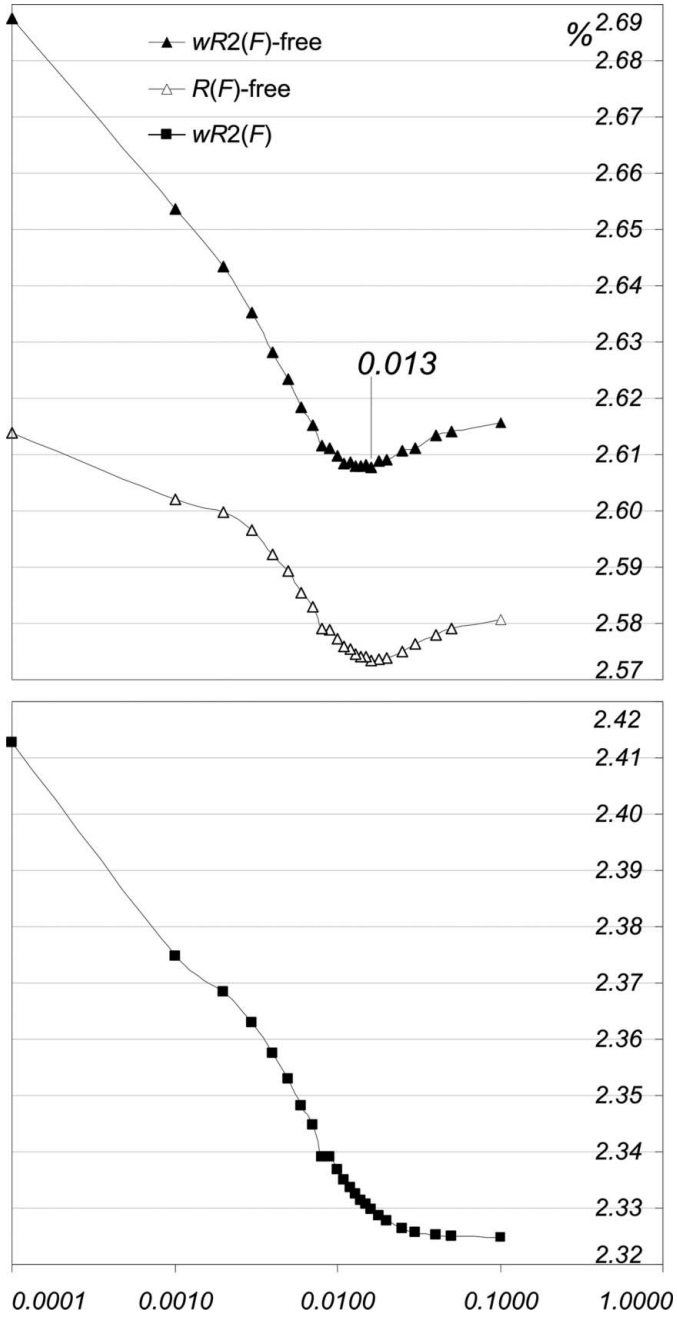

Figure 5
wR2(*F*), *R*(*F*)-free and *wR2*(*F*)-free values as a function of the allowed standard deviation applied to the chemical equivalence restraints (similarity of charge-density parameters κ, κ', P_{val}, P_{lm}).

4.2. Restraints and *R*-free calculations

Symmetry restraints have been applied most efficiently when the atomic local axes are optimized with respect to the atom local symmetry (Domagała & Jelsch, 2008). The local axes were generated automatically and are optimal in the present study. The similarity restraints, when applied to (κ, κ') values alone, led to very small variations in *R*-free values when different weights were applied. These changes were not significant and regular enough to observe a U-shaped curve and derive an optimal weight.

The average *R*-factors increase as expected when the weights of similarity or symmetry restraints were increased (Figs. 4 and 5). On the other hand, the averaged *wR2*(*F*)-free factors show a minimum at intermediate strengths of the restraints, around $\sigma_{Rsim} = 0.013$ for the charge-density similarity restraints and $\sigma_{Rsym} = 0.003$ for the atom local symmetry restraints. The *R*-free values are higher for very strong chemical equivalence restraints than for very weak restraints. In other words, according to the *R*-free test for the present charge-density study the refinement with no chemical equivalence constraints is better than the totally constrained refinement.

Alternatively, the application of local symmetry restraints yields a weighted *wR2*(*F*)-free minimum only slightly lower than the value of the strongly restrained refinement. This is less the case for the non-weighted free *R*-factor which leads to a more pronounced minimum at $\sigma_{Rsym} = 0.011$. For the local symmetry restraints, the constrained refinement is better than the non-constrained refinement.

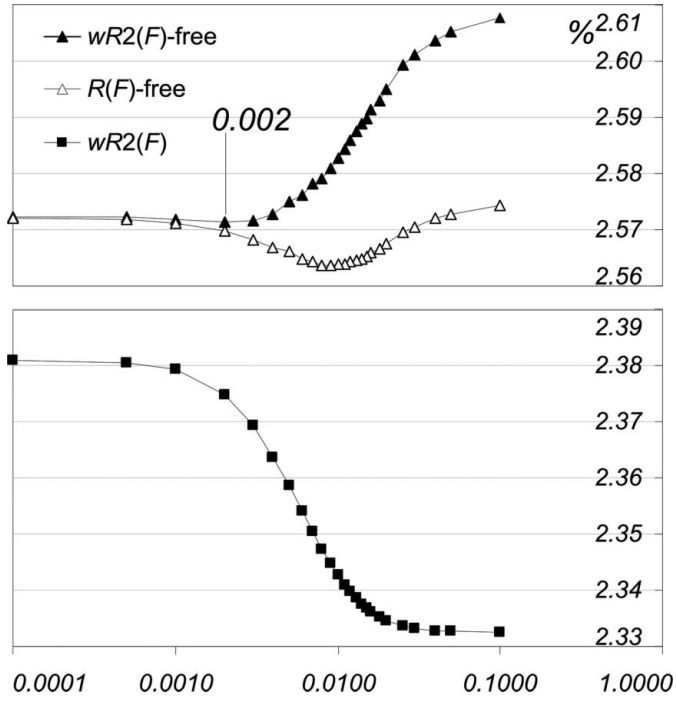

Figure 6
wR2(*F*), *R*(*F*)-free and *wR2*(*F*)-free values as a function of the allowed standard deviation of local symmetry restraints. The chemical equivalence (κ, κ', P_{val}, P_{lm} similarity) restraints are fixed at $\sigma_{Rsim} = 0.013$.

Table 5
Topological characteristics of the electron density at the covalent BCPs in 1-nitroindoline.

d is the bond length, r_1 and r_2 are the distances from the CP to the atoms defining the bond, ρ and $\nabla^2\rho$ denote the total electron density and its Laplacian, λ_1, λ_2, λ_3 are the principle curvatures, ε is the ellipticity and n_{topo} is the topological bond order. Values in italics in the second lines are from theoretical data.

Covalent bond	d (Å)	r_1 (Å)	r_2 (Å)	ρ (e Å^{-3})	$\nabla^2\rho$ (e Å^{-5})	λ_1	λ_2 (e Å^{-5})	λ_3	ε	n_{topo}
O1—N2	1.2596	0.6421	0.6175	3.1996	−8.65	45.98	−26.36	−28.27	0.07	1.82
	1.2428	*0.6308*	*0.6120*	*3.0722*	*−7.75*	*41.48*	*−23.24*	*−25.99*	*0.11*	*1.73*
O2—N2	1.2354	0.6262	0.6093	3.3171	−11.5	44.95	−27.67	−28.78	0.04	1.86
	1.2406	*0.6309*	*0.6096*	*3.1093*	*−8.57*	*41.35*	*−23.78*	*−26.14*	*0.09*	*1.74*
N1—N2	1.3672	0.6742	0.6931	2.4862	−8.35	32.48	−17.75	−23.08	0.23	1.42
	1.3409	*0.6564*	*0.6845*	*2.4692*	*−8.11*	*30.84*	*−16.67*	*−22.28*	*0.25*	*1.51*
N1—C1	1.4149	0.8205	0.5955	1.8751	−11.97	15.06	−12.64	−14.39	0.12	0.86
	1.4163	*0.8222*	*0.5951*	*1.8243*	*−11.06*	*13.82*	*−11.58*	*−13.30*	*0.13*	*0.85*
N1—C7	1.503	0.8474	0.6556	1.6284	−6.15	16.12	−10.7	−11.57	0.08	0.70
	1.4767	*0.8476*	*0.6292*	*1.5676*	*−5.39*	*15.29*	*−10.03*	*−10.65*	*0.06*	*0.66*
C1—C2	1.4368	0.7385	0.6983	2.0127	−16.25	11.72	−12.69	−15.29	0.17	1.27
	1.4033	*0.7276*	*0.6758*	*2.0572*	*−17.25*	*10.11*	*−12.30*	*−15.07*	*0.18*	*1.41*
C2—C3	1.3917	0.7060	0.6858	2.0967	−17.94	11.22	−13.33	−15.83	0.16	1.33
	1.3876	*0.7064*	*0.6813*	*2.0872*	*−18.07*	*10.04*	*−12.62*	*−15.50*	*0.19*	*1.40*
C3—C4	1.4175	0.6878	0.7297	2.0488	−16.34	11.7	−12.88	−15.16	0.15	1.35
	1.3991	*0.7005*	*0.6986*	*2.0315*	*−16.46*	*11.00*	*−12.48*	*−14.98*	*0.17*	*1.36*
C4—C5	1.4312	0.732	0.6992	2.0618	−16.34	11.48	−12.7	−15.12	0.16	1.41
	1.3959	*0.6990*	*0.6969*	*2.0499*	*−16.58*	*10.92*	*−12.48*	*−15.02*	*0.17*	*1.40*
C5—C6	1.4063	0.7095	0.6968	2.0489	−16.38	10.96	−12.62	−14.72	0.14	1.42
	1.4000	*0.6963*	*0.7038*	*2.0364*	*−16.04*	*10.83*	*−12.28*	*−14.59*	*0.16*	*1.44*
C1—C6	1.4131	0.7295	0.6838	2.0827	−17.25	11.42	−12.95	−15.72	0.18	1.36
	1.3952	*0.7288*	*0.6668*	*2.0568*	*−16.94*	*10.61*	*−12.40*	*−15.15*	*0.18*	*1.40*
C2—C8	1.5212	0.7573	0.7641	1.622	−9.33	12.09	−10.38	−11.04	0.06	1.03
	1.5083	*0.7703*	*0.7382*	*1.6194*	*−9.04*	*11.81*	*−10.07*	*−10.78*	*0.07*	*1.08*
C8—C7	1.5601	0.7665	0.7936	1.5443	−7.33	12.88	−10.07	−10.14	0.01	0.99
	1.5410	*0.7571*	*0.7840*	*1.5002*	*−6.27*	*13.26*	*−9.75*	*−9.78*	*0.00*	*0.96*

The restraint weight leading to the lowest *R*-free values depends on the weighting scheme used. In an initial refinement *versus* *F* with $W = 1/\sigma_F^2$, the best *wR*2(*F*) free values were obtained with $\sigma_{restrain}$ = 0.006 for the equivalence of both atoms and local symmetry restraints.

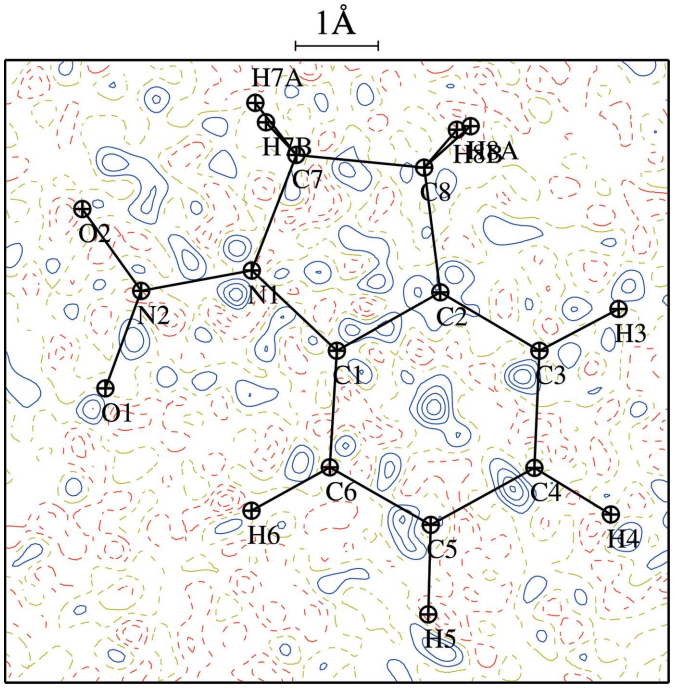

Figure 7
Residual electron density in the main plane at sin $\theta/\lambda < 1.2$ Å^{-1} and $I/\sigma_I > 1$. Contour intervals 0.05 Å^{-3}; solid lines represent positive contours, dashed lines represent negative contours and yellow dashed lines are zero contours.

The charge-density similarity and symmetry restraints were then combined together, σ_{Rsim} was fixed at 0.013, its optimal value, while σ_{Rsym} was varied. The combined restraint (Fig. 6) gives similar trends of *R* and *R*-free factors as a function of symmetry restraint weight as in Fig. 5. The lowest *R*-free value is achieved for a symmetry restraint with σ_{Rsym} = 0.002; this value together with σ_{Rsym} = 0.013 was used in the multipolar refinement SCA5. The lowest average *R*-free value obtained is slightly better for the combination of both types of restraints [*wR*2(*F*)-free = 0.0257] than for the similarity (0.0261) or symmetry restraints (0.0259) alone. The numbers compared here show very small differences, but the regularity of the curves (average *R*-free as a function of $\sigma_{restrain}$) suggests that the comparisons are meaningful. In the average free *R*-factors, each reflection is taken into account once. On the contrary, the individual free *R*-factors show much larger deviations, reaching an absolute value of 0.3% in a sample of 20 different refinements (supplementary material, Fig. Sup. 3).

Two models for H atoms were tested. In the U_{iso} model the displacement parameters of the H atoms were isotropic and ride on the U_{eq} of the bonded atom: $U_{iso} = 1.2*U_{eq}$. In the anisotropic model the displacement parameters are fixed to those calculated by the rigid-body analysis of *THMA* (Trueblood, 1978) applied by the *SHADE* server (Madsen *et al.*, 2004). The number of variables is the same in the two models. The *R*-free and *R*-factors are both systematically lower (by $\sim$ 0.025 and $\sim$ 0.03% in absolute value) with the anisotropic

model than with the isotropic model. This is in agreement with the study of Hoser *et al.* (2009) which recommends the use of estimated anisotropic atomic displacement parameters as the best model for H atoms in experimental charge-density refinement when no neutron diffraction data are available. The final refinement was therefore carried out with these fixed U_{ani} parameters for H atoms.

4.3. Electron density

A two-dimensional residual Fourier electron-density map (Fig. 7) was computed using 4043 independent reflections with $\sin\theta/\lambda < 0.9$ Å^{-1} and $I/\sigma_I > 1$. The residual densities in the two-dimensional map are featureless and are in the range -0.17 to $+0.23$ e Å^{-3}.

Static deformations maps in the two main planes of the molecule for experimental and theoretical data are depicted in Fig. 8. The electron density is apparently well modeled by the multipole expansion. The highest deformation feature is at 1.35 e Å^{-3} for theoretical data and at 1.896 e Å^{-3} for experimental data in the plane of the nitramino group. The experimental and theoretical deformation maps remain in good agreement and display the expected bonding features. The deformation electron density for the nitro group and aromatic ring generally follows the local symmetries of the atoms. The strong polarization of C—N and N—O bonds in the direction of the N atom is clearly visible, while the N—N bond appears to be non-polar. This pattern is typically observed for *N*-nitro compounds (Zhurova *et al.*, 2007) and for nitro groups (Zhurova & Pinkerton, 2001). The two electron lone pairs of the two nitro oxygens are noticeable, with an N—O—lp angle close to 90°, as observed in a previous study (Kubicki *et al.*, 2002). Both theoretical and experimental maps show strong local depletion near the oxygen nucleus along the N—O bond. The static deformation electron-density grids obtained from theoretical and experimental multipole modeling display a correlation coefficient of 87% and a root mean square (r.m.s.) quotient of 0.92.

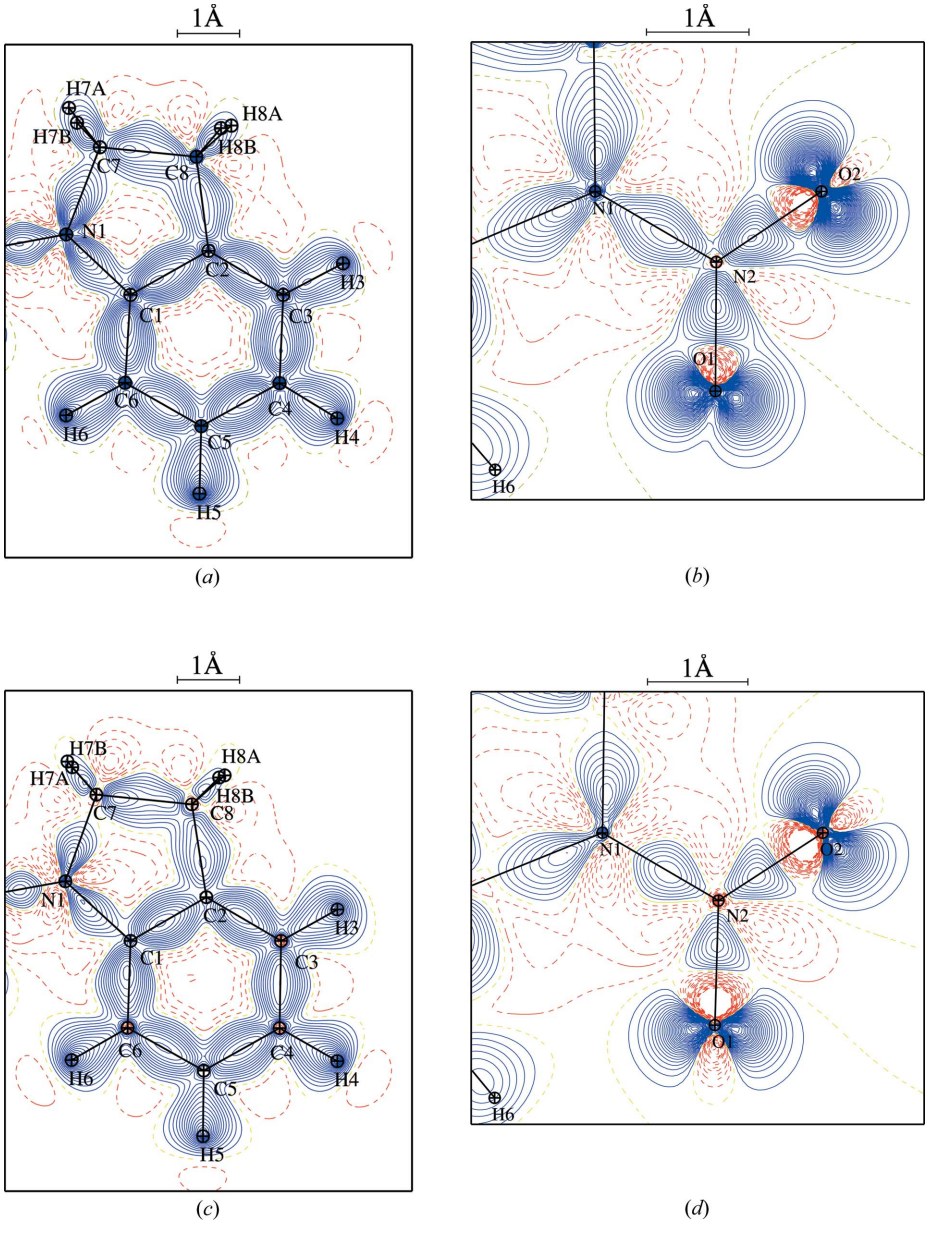

Figure 8
Static deformation electron-density maps in the two main planes of 1-nitroindoline; (*a*) and (*b*) for experimental data; (*c*) and (*d*) for theoretical data. Contour intervals as in Fig. 7, blue solid lines represent positive contours, red dashed lines represent negative contours and yellow dashed lines are zero contours.

4.4. Topology of covalent and hydrogen bonds

The BCP topological parameters are summarized in Table 5. The standard uncertainty on the second derivatives, the Laplacian and ellipticities of the electron density is estimated to be $\sim 10\%$ of their values (Espinosa *et al.*, 1999). All chemical bonds of the 1-nitroindoline crystal are characterized by (3,−1) BCPs. The experimental and theoretical values are in good agreement. The BCP electron densities, Laplacian values and corresponding bond lengths show the expected consistency. The value of the Laplacian is stronger for the N1—C1 bond (−11.97 and −11.06 e Å^{-5} for experimental

Table 6
Topological characteristics of the electron density at all the hydrogen BCPs and O2···O2^{iii} short contact in 1-nitroindoline.

G^{CP}, V^{CP} and E^{CP} are the kinetic, potential and total electronic energies (Abramov, 1997) at CPs; D_e is the dissociation energy. See Table 5 for a detailed description. Values in italics are from theoretical data.

Bond	d (Å)	r_1 (Å)	r_2 (Å)	ρ (e Å^{-3})	$\nabla^2\rho_{cp}$ (e Å^{-5})	λ	λ_2 (e Å^{-5})	λ_3	ε	G^{CP}	V^{CP} (kJ mol^{-1} bohr^{-3})	E^{CP}	D_e (kJ mol^{-1})
H6···O1	2.3057	1.3160	1.0047	0.1007	1.53	2.28	−0.37	−0.37	0.00	34.60	−27.50	7.10	−13.75
	2.3325	*1.3189*	*1.0402*	*0.0990*	*1.54*	*2.28*	*−0.36*	*−0.38*	*0.04*	*34.60*	*−27.20*	*7.40*	*−13.60*
H5···O1^{i}	2.6557	1.5091	1.1644	0.0363	0.60	0.83	−0.12	−0.12	0.04	12.10	−7.90	4.20	−3.95
	2.7912	*1.5538*	*1.2768*	*0.0291*	*0.51*	*0.67*	*−0.08*	*−0.09*	*0.04*	*10.00*	*−6.30*	*3.70*	*−3.15*
H6···O1^{i}	2.8520	1.5801	1.2841	0.0266	0.42	0.56	−0.06	−0.07	0.19	8.50	−5.30	3.20	−2.65
	2.7264	*1.5348*	*1.2421*	*0.0301*	*0.55*	*0.74*	*−0.09*	*−0.10*	*0.09*	*10.80*	*−6.80*	*4.00*	*−3.40*
H7*B*···O1^{ii}	2.4531	1.3985	1.0856	0.0662	0.94	1.42	−0.23	−0.25	0.08	20.40	−15.30	5.10	−7.65
	2.5209	*1.4065*	*1.1287*	*0.0690*	*0.94*	*1.39*	*−0.23*	*−0.23*	*0.00*	*20.70*	*−15.80*	*4.90*	*−7.90*
H3···O2^{iii}	2.4990	1.4470	1.0638	0.0502	0.81	1.16	−0.17	−0.18	0.02	16.80	−11.60	5.20	−5.80
	2.6036	*1.4614*	*1.1879*	*0.0388*	*0.80*	*1.09*	*−0.14*	*−0.15*	*0.02*	*15.90*	*−10.00*	*5.90*	*−5.00*
O2···O2^{iv}	2.8304	1.4153	1.4151	0.0732	1.21	1.59	−0.13	−0.25	0.49	26.00	−19.00	7.00	−9.50
	2.8708	*1.4355*	*1.4353*	*0.0677*	*1.13*	*1.48*	*−0.13*	*−0.22*	*0.42*	*24.00*	*−17.30*	*6.70*	*−8.65*

Symmetry transformations used to generate equivalent atoms: (i) $1-x, 2-y, -z$; (ii) $1+x, y, z$; (iii) $x, -1+y, -1+z$; (iv) $2-x, 2-y, 1-z$.

and theoretical data) than on the N1—C7 bond. This may denote the partial π character of the N1—C1 bond suggesting an overlap between the π-electron systems between the aromatic ring and the nitramino group. The total electron density at the C—C bond CPs in the aromatice ring shows an alternation of values slightly above and below the average value, which is consistent with a difference in their bond lengths. The same trend was found for the total charge density derived from the theoretical diffraction data. The theoretical and experimental Laplacian values at the BCPs are highly correlated (98.5%) and display similar magnitudes (13.6 and 13.1 e Å^{-5}). There are some discrepancies for the ellipticity values, particularly for the nitro group. Data derived from theoretical calculations suggest the partial double-bond character of the N—O bond, which is consistent with the resonance scheme and electron delocalization on the nitramino group. Nevertheless, the high value of ellipticity for the N1—N2 bond (0.23 and 0.25 for experimental and theoretical calculations) implies a major influence of the mesomeric form with a double N═N bond along with a positively charged N2 atom and negatively charged O atoms. This corresponds well with the monopole charges $\delta = N_{val} - P_{val}$ derived from experimental as well as theoretical data after multipolar and kappa refinements ($\delta_{O1} = -0.213$, $\delta_{O2} = -0.206$, $\delta_{N2} = +0.060$ from experiment; $\delta_{O1} = -0.201$, $\delta_{O2} = -0.250$, $\delta_{N2} = +0.139$ from theoretical data). Nevertheless, the final estimation of the bond order can be taken from the topological bond order (n_{topo}) calculation. The approximation of the n_{topo} values was introduced by Howard & Lamarche (2003) with the expression

$$n_{topo} = a + b\lambda_1 + c(\lambda_2 + \lambda_3) + d\rho, \qquad (4)$$

where λ_1, λ_2, λ_3 are the electron density curvatures (in atomic units), ρ is the electron density (in atomic units) at the CP (critical point) and a, b, c, d are coefficients obtained from molecular theoretical calculations by the fit of equation (4) to the Cioslowski & Mixon (1991) bond orders. In the present analysis the following parameters were used: for the N—N bonds $a = -0.775$, $b = 0.525$, $c = 2.041$, $d = 13.432$; for the N—O bonds $a = -0.628$, $b = 0.505$, $c = 0.448$, $d = 5.275$; for the C—C bonds $a = -1.004$, $b = 0.634$, $c = 2.839$, $d = 17.633$; for C—N bonds $a = -0.851$, $b = 0.221$, $c = 0.715$, $d = 8.561$ (Chen *et al.*, 2007; Zhurova *et al.*, 2006). The calculated topological bond orders (Table 5) are consistent with previous publications devoted to explosive nitro compounds (Chen *et al.*, 2007; Zhurova *et al.*, 2006, 2007). The partial π character of the N1—C1 bond has not been confirmed. The value of 0.87 (0.85 for theoretical data) excludes overlap between the π-electron systems of the aromatic ring and the nitramino fragment. Parameters for the remaining bonds are consistent with previous analyses. The average N—O and N—N bond orders are 1.84 and 1.42 (1.74 and 1.51 for theoretical data), reflecting the overlap of the electron density in the $-N_2O_2$ group. As anticipated, the C—C bonds of the aromatic residue show bond-order values between 1.27 and 1.44 typical for delocalized bonds. The C7—C8 bond between two Csp^3 atoms has a bond order close to one.

Significant hydrogen bonding is present in the crystal structure. Based on energy criteria, careful examination of the intermolecular space for additional interactions has been carried out, resulting in three hydrogen bonds (Table 6) compared with the previous structural study (Zaleski *et al.*, 2001). On each bond path between the hydrogen and acceptor atoms, there is a critical point of the type (3,−1) (Table 6). The presence of a BCP along with other geometrical parameters is a Koch & Popelier (1995) condition for the existence of a polar non-bonded interaction of the H···*A* type (Bader, 1990). The hydrogen bonds are relatively weak as they are of the C—H···O type. The C6—H6···O1 interaction is internal to the molecule and generates a six-membered ring. From a geometrical point of view, the C6—H6···O1 hydrogen bond with a $\angle(DHA)$ angle value of 110.84° is the weakest; it was not reported in the room-temperature study (Zaleski *et al.*, 2001). Nevertheless, the presence of the ring critical point [RCP, (3,+1)] in the middle of the cycle generated by the N1—C1—C6—H6···O1—N2 atoms ($\rho = 0.0622$ e Å^{-3}; $\nabla^2\rho = 1.58$, $\lambda_1 = 1.24$, $\lambda_2 = 0.50$, $\lambda_3 = -0.16$ e Å^{-3}; ellipticity = 0.60) further validates its presence. The total electron density along with

energy density characteristics (Abramov, 1997) at the CP is higher compared with the remaining intermolecular hydrogen bonds (Table 6).

The estimated values of the energies can be obtained from the properties at the CPs. The approximate energies of stabilization may be derived from the equation

$$D_e = -a_0^3 \cdot V^{CP}/2, \quad (5)$$

where a_0 is the Bohr radius and V^{CP} is the value of the potential energy at the CP (Espinosa & Molins, 2000). The experimental values correlate well with the corresponding theoretical data. The strongest hydrogen bond is also the intramolecular C6—H6···O1 hydrogen bond when D_e values are considered. The interaction C7—H7*B*···O1^{ii} [symmetry code: (ii) $1 + x, y, z$] is the strongest intermolecular hydrogen bond in the structure. Among the intermolecular interactions, the O···O contact has the highest estimated dissociation energy. The contact as mentioned above is typical for nitro compounds and especially for explosive ones. Its energy is comparable with the value obtained for typical energetic materials (Chen *et al.*, 2007). Unfortunately, there are only a few values published for these non-hydrogen-bonding weak interactions. Examination of the energies is important as they could be helpful in predicting the mechanism of initial decomposition for explosive materials (Zhurova *et al.*, 2004).

4.5. Charge density and restraints

The r.m.s. deviation of the charge-density parameters subject to symmetry and chemical equivalence restraints were evaluated after refinement with and without applying the corresponding restraints. The multipoles which are not compatible with a local symmetry (*e.g.* those which are anti-symmetric with respect to a mirror plane) are expected to be small in a charge-density refinement. The r.m.s value of these multipoles, which reflects the global deviation from symmetry, is 0.020 and 0.011 for the unrestrained and restrained refinements. The r.m.s. deviation of (P_{val} and P_{lm}) type parameters with respect to the chemical equivalences are 0.029 and 0.012 for the unrestrained and restrained refinement.

The electron lone pairs of the O atoms were specially studied with respect to application of the local symmetry restraints. The lone-pair electron densities require a higher resolution to be well observed as they generally are more concentrated in space than the bonding density. This can be seen both in the deformation maps and in the κ' coefficients. The multipoles which model the bonding density of the C and N atoms are on average ($\langle\kappa'\rangle$ = 0.91 for the present compound) less contracted than those of the O atoms ($\langle\kappa'\rangle$ = 1.18). The refined experimental electron density of the lone pairs is therefore more sensitive than the bonding density to diffraction data measurement errors, limited resolution or high atomic *B* factors. The nitro group, as it is not strongly polarizable (Jin *et*

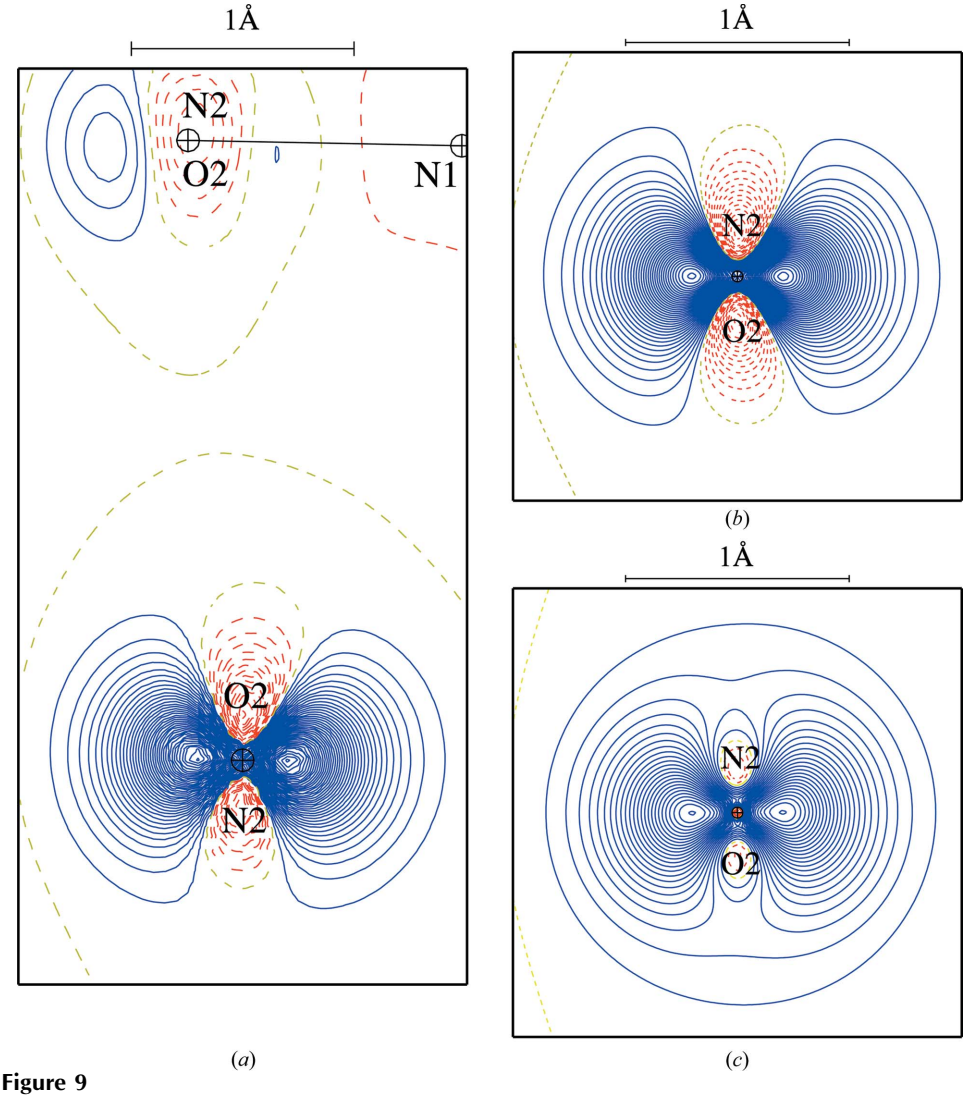

Figure 9
Static deformation electron-density maps showing the electron lone pairs for the O2 atom of the nitro group. The views are in the planes containing the O atom and perpendicular to the N2—O2 bond. (*a*) Experimental map, without symmetry and chemical equivalence restraints. (*b*) Experimental map with optimally weighted symmetry and chemical equivalence restraints. (*c*) Theoretical data refinement without restraints. Contour intervals as in Fig. 7, blue solid lines represent positive contours, red dashed lines represent negative contours and yellow dashed lines are zero contours.

al., 2006), is expected to have an electron density which is essentially symmetric with respect to the NO_2 plane. The theoretical density (Fig. 9*c*) is indeed very symmetric with respect to the nitro sp^2 plane: the r.m.s. value of multipoles antisymmetric to the nitro plane is 0.001 while the uncertainty is 0.005.

In the experimental refinement SCA5 without charge-density symmetry restraints, the r.m.s. value of the six multipoles which are antisymmetric to the nitro group plane reaches 0.016 and 0.012 for atoms O1 and O2. For reference, the average uncertainty on the experimental multipoles of the O atoms is 0.004 for the refinement without symmetry and chemical equivalence restraints. The deviations from symmetry are therefore typically between three and four times the standard uncertainty for the unrestrained refinement. The electron lone pairs of atoms O1 and O2 show a visible deviation from symmetry; the line going through the two lobe centers of the lone pairs deviates by a 2 and 3° rotation from the nitro group mirror plane in the symmetry unrestrained refinement (Fig. 9*b*). The short O2···O2 contact (Table 6) could have an influence on the electron density of the O2 atom and explain this dissymmetry (Fig. 3 and Fig. 9*b*).

However, in the refinement with optimal symmetry restraints, the deviation from symmetry with respect to the sp^2 nitro plane is significantly reduced. The lines between the centers of the electron lone pairs of the O1 and O2 atoms show an angle deviation which is reduced to 0 and 0.5°. The r.m.s. values of the antisymmetric multipoles are reduced to 0.002 and 0.0012 for the O1 and O2 atoms, which are similar and lower than the standard uncertainty. The small deviation from symmetry of the O-atom lone pairs can therefore be attributed to experimental errors and uncertainties. This is consistent with the quantum calculations which do not produce such dissymmetry.

5. Conclusions

The charge-density distribution in the crystal of 1-nitroindoline has been experimentally determined by means of high-resolution X-ray diffraction. There are four weak C—H···O hydrogen bonds involving the nitro group. The crystal packing displays a remarkable O2···O2 intermolecular contact which is shorter than the van der Waals interaction and where two nitro groups stack together around an inversion center. No critical differences among structures obtained from data collected at room and low temperature are observed. *R*-free analyses were performed involving a series of comprehensive refinements using different weighting schemes for charge-density similarity and symmetry restraints. The results of these tests imply that the comparisons are meaningful. Two models for H atoms were tested: the U_{iso} model and the anisotropic model calculated by the rigid-body analysis of *THMA* (Trueblood, 1978). The restraint weights with the lowest average *R*-free factors and the anisotropic H-atom model were applied in the final refinement. This approach yielded a well modeled electron-density distribution of the molecule which is comparable to that obtained from the theoretical computations. The static deformation electron density grids obtained from theoretical and experimental multipole modeling display a correlation coefficient of 87% and a root mean-square (r.m.s.) quotient of 0.92. The experimental charge density from the refinement with no symmetry restraints on the multipoles reveals that the electron lone pairs of the O2 atom show a visible deviation from symmetry with respect to the nitro group plane. Despite the presence of a short O2···O2 contact, this asymmetry is not confirmed by theory or refinement with the appropriate symmetry restraints.

The electron density within the N_2O_2 group was found to involve the major influence of the mesomeric form of the N=N double bond along with the positively charged N2 atom and negatively charged nitro O atoms. The topology of electron density suggests a lack of conjugation between the π-electron systems of the aromatic ring and the nitramino group which was not so obvious in previous investigations.

The present study suggests that appropriate weighting applied to the charge-density restraints can reduce observed artefacts and make the final result physically reliable and meaningful. The proposed approach can be considered to be a novel method of evaluation of the restrained charge-density model, especially in view of future applications in high-resolution protein crystallography.

Nancy University is thanked for an invited assistant professor position granted to Bartosz Zarychta. Sebastien Lebegue is thanked for technical help.

References

Abrahams, S. C. & Keve, E. T. (1971). *Acta Cryst.* A**27**, 157–165.
Abramov, Yu. A. (1997). *Acta Cryst.* A**53**, 264–272.
Allen, F. H., Kennard, O., Watson, D., Brammer, L., Orpen, A. & Taylor, R. (1992). *International Tables for Crystallography*, Vol. C, ch. 9.5, pp. 685–706. Dordrecht: Kluwer Academic Publishers.
Anulewicz, R., Krygowski, T. M., Gawinecki, R. & Rasala, D. (1993). *J. Phys. Org. Chem.* **6**, 257–260.
Bader, R. F. W. (1990). *Atoms in Molecules: a Quantum Theory*. Oxford: Clarendon Press.
Blessing, R. H. (1995). *Acta Cryst.* A**51**, 33–38.
Brünger, A. T. (1992). *Nature*, **355**, 472–475.
Brünger, A. T. (1993). *Acta Cryst.* D**49**, 24–36.
Brzózka, L., Baran, W., Kraus, W. & Tomasik, P. (1995). *Pol. J. Chem.* **69**, 605–611.
Chen, Y.-S., Stash, A. I. & Pinkerton, A. A. (2007). *Acta Cryst.* B**63**, 309–318.
Cioslowski, J. & Mixon, S. T. J. (1991). *J. Am. Chem. Soc.* **113**, 4142–4145.
Clementi, E. & Roetti, C. (1974). *At. Data Nucl. Data Tables*, **14**, 177–478.
Daszkiewicz, Z., Kyzioł, J. B., Prezdo, W. W. & Zaleski, J. (2000). *J. Mol. Struct.* **553**, 9–18.
Daszkiewicz, Z., Zaleski, J., Nowakowska, E. M. & Kyziol, J. B. (2002). *Pol. J. Chem.* **76**, 1113–1125.
Domagała, S. & Jelsch, C. (2008). *J. Appl. Cryst.* **41**, 1140–1149.
Dovesi, R., Saunders, V. R., Roetti, C., Orlandol, R., Zicovich-Wilson, C. M., Pascale, F., Civalleri, B., Doll, K., Harrison, N. M., Bush, I. J., D'Arco, Ph. & Llunell, M. (2008). *CRYSTAL*06, Version 1.0.2. University of Turin, Italy.
Ejsmont, K., Kyzioł, J., Daszkiewicz, Z. & Bujak, M. (1998). *Acta Cryst.* C**54**, 672–674.

Espinosa, E. & Molins, E. J. (2000). *Chem. Phys.* **113**, 5686–5694.
Espinosa, E., Souhassou, M., Lachekar, H. & Lecomte, C. (1999). *Acta Cryst.* B**55**, 563–572.
Gavezzotti, A. (2010). *Acta Cryst.* B**66**, 396–406.
Growenlock, B. G., Pfab, J. & Young, V. M. (1997). *J. Chem. Soc. Perkin Trans. 2*, pp. 915–919.
Guillot, B., Viry, L., Guillot, R., Lecomte, C. & Jelsch, C. (2001). *J. Appl. Cryst.* **34**, 214–223.
Hansen, N. K. & Coppens, P. (1978). *Acta Cryst.* A**34**, 909–921.
Hariharan, P. C. & Pople, J. A. (1973). *Theor. Chim. Acta*, **28**, 213–222.
Hohenberg, P. & Kohn, W. (1964). *Phys. Rev. B*, **136**, 864–871.
Hoser, A. A., Dominiak, P. M. & Woźniak, K. (2009). *Acta Cryst.* A**65**, 300–311.
Howard, S. T. & Lamarche, O. (2003). *J. Phys. Org. Chem.* **16**, 133–141.
Jelsch, C., Guillot, B., Lagoutte, A. & Lecomte, C. (2005). *J. Appl. Cryst.* **38**, 38–54.
Jin, P., Murray, J. S. & Politzer, P. (2006). *Int. J. Quantum Chem.* **106**, 2347–2355.
Koch, U. & Popelier, P. L. A. (1995). *J. Phys. Chem.* **99**, 9747–9754.
Kubicki, M., Borowiak, T., Dutkiewicz, G., Souhassou, M., Jelsch, C. & Lecomte, C. (2002). *J. Phys. Chem. B*, **106**, 3706–3714.
Lee, C., Yang, W. & Parr, R. G. (1988). *Phys. Rev. B*, **37**, 785–789.
Madsen, A. Ø., Sørensen, H. O., Flensburg, C., Stewart, R. F. & Larsen, S. (2004). *Acta Cryst.* A**60**, 550–561.
Mialocq, J. C. & Stephenson, J. C. (1986). *Chem. Phys.* **106**, 281–291.
Oxford Diffraction (2002*a*). *CrysAlis CCD*. Oxford Diffraction Ltd, Abingdon, England.
Oxford Diffraction (2002*b*). *CrysAlis RED*. Oxford Diffraction Ltd, Abingdon, England.
Oxford Diffraction Ltd (2006). *SCALE3 ABSPACK, CrysAlis Software Package*. Oxford Diffraction Ltd, Abingdon, England.
Pinkerton, A. A. & Ritchie, J. P. (2003). *J. Mol. Struct.* **657**, 57–74.
Ridd, J. H. & Scriven, E. F. V. J. (1972). *J. Chem. Soc. Chem. Commun.* **11**, 641.
Sarazin, Y., Howard, R. H., Hughes, D. L., Humphrey, S. M. & Bochmann, M. (2006). *Dalton Trans.* pp. 340–350.
Schomaker, V. & Trueblood, K. N. (1998). *Acta Cryst.* B**54**, 507–514.
Sheldrick, G. M. (2008). *Acta Cryst.* A**64**, 112–122.
Stewart, R. F., Davidson, E. R. & Simpson, W. T. (1965). *J. Chem. Phys.* **42**, 3175–3187.
Trueblood, K. N. (1978). *Acta Cryst.* A**34**, 950–954.
Volkov, A., Abramov, Y. A. & Coppens, P. (2001). *Acta Cryst.* A**57**, 272–282.
Volkov, A., Gatti, C., Abramov, Y. & Coppens, P. (2000). *Acta Cryst.* A**56**, 252–258.
White, W. N., Hathaway, C. & Huston, D. (1970). *J. Org. Chem.* **35**, 737–739.
Williams, D. H. L. (1982). *The Chemistry of Amino, Nitroso and Nitro Compounds and Their Derivatives.* Chichester: Wiley.
Wright, G. F. (1969). *The Chemistry of the Nitro, Nitroso and Amino Groups*, pp. 614–683. Chichester: J. Wiley and Sons.
Zaleski, J., Daszkiewicz, Z. & Kyzioł, J. B. (1999). *Acta Cryst.* C**55**, 1292–1295.
Zaleski, J., Daszkiewicz, Z. & Kyzioł, J. B. (2001). *Acta Cryst.* C**57**, 304–305.
Zarychta, B., Pichon-Pesme, V., Guillot, B., Lecomte, C. & Jelsch, C. (2007). *Acta Cryst.* A**63**, 108–125.
Zhurova, E. A. & Pinkerton, A. A. (2001). *Acta Cryst.* B**57**, 359–365.
Zhurova, E. A., Stash, A. I., Tsirelson, V. G., Zhurov, V. V., Bartashevich, E. V., Potemkin, V. A. & Pinkerton, A. A. (2006). *J. Am. Chem. Soc.* **128**, 14728–14734.
Zhurova, E. A., Tsirelson, V. G., Stash, A. I., Yakovlev, M. V. & Pinkerton, A. A. (2004). *J. Phys. Chem. B*, **108**, 20173–20179.
Zhurova, E. A., Zhurov, V. V. & Pinkerton, A. A. (2007). *J. Am. Chem. Soc.* **129**, 13887–13893.
Zhurov, V. V., Zhurova, E. A. & Pinkerton, A. A. (2008). *J. Appl. Cryst.* **41**, 340–349.